Hindawi
International Journal of Aerospace Engineering
Volume 2020, Article ID 8837564, 13 pages
https://doi.org/10.1155/2020/8837564

Research Article

Prediction of High-Cycle Fatigue Performance of 1Cr11Ni2W2MoV Stainless Steel Plate after Foreign Object Damage

Zhenhua Zhao,[1] **Lingfeng Wang**,[1] **Chao Liu**,[2] **Lulu Liu**,[1] **and Wei Chen**[1]

[1]*Aero-Engine Thermal Environment and Structure Key Laboratory of Ministry of Industry and Information Technology, College of Energy and Power Engineering, Nanjing University of Aeronautics and Astronautics, Nanjing 210016, China*
[2]*Jiangsu Aero-XY Technology Co., Ltd., Wuxi 214000, China*

Correspondence should be addressed to Wei Chen; chenwei@nuaa.edu.cn

Received 6 June 2020; Revised 8 September 2020; Accepted 5 October 2020; Published 19 October 2020

Academic Editor: Marco Pizzarelli

High-cycle fatigue (HCF) properties of 1Cr11Ni2W2MoV stainless steel impacted by a high-speed steel ball were studied by the foreign object damage (FOD) test and HCF test. The results show that the damage depth Z has the most obvious effect on the HCF limit of notched flat plate specimens, and the fatigue limit decreases with the increase of depth Z. The microcharacteristics of the FOD notch and HCF fracture of 1Cr11Ni2W2MoV stainless steel were observed by a scanning electron microscope (SEM). The results show that the microdamage features such as plastic deformation, loss of material, and microcracks promote the initiation and propagation of fatigue cracks, and the fatigue source area lies near the root of the notch. The Peterson formula and Worst Case Notch (WCN) mode were used to predict the HCF limit of flat plate specimens after FOD. The crack growth threshold was obtained by the crack growth test. The results show that the prediction results of both methods are conservative. For the notch with damage depth $Z < 1$ mm, the prediction accuracy of the WCN model is higher (error range < 30%). For the notch with damage depth $Z > 1$ mm, the prediction results of both methods have large errors (>30%) with the WCN model being slightly more accurate.

1. Introduction

During the service of aeroengine, it is unavoidable to draw nearby particles into the flow path of the engine, including birds, ice, and small hard objects. The impact of birds and ice belongs to soft impact, namely, bird strike [1] and ice impact [2], and the impact of small hard objects such as bolts, nuts, sand, and stones is called foreign object damage (FOD) [3]. FOD often occurs near the ground during the operation, forming a dent or notch at the leading edge of the blade [4]. FOD has become a key issue which must be considered in the design of aeroengine blades.

The FOD on aeroengine blades is a complex transient dynamic problem, which involves the nonlinearity, contact, and large deformation of materials. Many scholars have paid more and more attention to FOD in recent years. The most intuitive way to study the FOD problem is to test the impact damage prefabricated. The most used method is the air cannon method [5]. Peters et al. [6] used an air cannon to launch steel balls to impact the surface of the Ti-6A1-4V plate and observed the bottom of the notch by a scanning electron microscope (SEM) and found obvious microcrack damage caused by high-speed impact. Farahani et al. [7] carried out ballistic impact tests by air cannon, launching steel foreign objects of different shapes on Udimet-500 nickel-based alloy (the first-stage rotor material of the Fiat gas turbine engine) with different impact velocities and incident angles. The result shows that there are many microcracks at the damage caused by cube foreign object incident at a 45° angle. Bache et al. [8] conducted FOD tests using ballistic systems. The Ti-6A1-4V plate samples were impacted with 2 mm diameter steel balls at different incident speeds. The

results show that there are ductile indentations at the impact position under low energy impacts, while loss of material (LOM) was observed on the edge of damaged samples under high energy impacts.

With the development of finite element analysis technology, the process of simulating the impact of foreign objects on the blade by finite element software has also become a common method in studying FOD. Oakley and Nowell [9] and Duó et al. [10] used software such as LS-DYNA, DYTRAN, ABAQUS, and material models such as Bammann and Johnson-Cook to perform dynamic simulation analysis for the foreign object impacting process. The damage morphology obtained by the simulation is in good agreement with the experimental results, which proves the applicability of simulation analysis on blade FOD. Chen and Hutchinson [11] used ABAQUS finite element software to simulate the process of steel ball striking the edge of the Ti-6A1-4V flat plate. After studying the residual stress distribution at the FOD location, it was found that a significant residual tension area is formed at the raised tip at the bottom of the notch due to lateral expansion and then resulted in fatigue cracks. Marandi et al. [12] used the finite element method and the experimental method to investigate the stress concentration factor at the notch root of the turbine blade leading edge. The results showed that the finite element calculation results agree well with the experimental data.

Aeroengine blades are subjected to high-cycle fatigue (HCF) loads caused by vibration and short-time resonance during operation. Stress concentrations, residual stresses, and microscopic damage at the FOD location will accelerate the initiation of cracks under HCF, resulting in premature fatigue damage to engine blades in its designed cycles. That means FOD is an important factor limiting the high-cycle fatigue performance of engine blades [13]. Ruschau et al. [14] performed high-cycle fatigue tests on Ti-6Al-4V blades which were impacted by glass beads at different incident angles. Bache et al. [8] studied the effects of different foreign object sizes and shapes on the fatigue strength of the FOD flat specimen. Martinez et al. [15] performed high-cycle fatigue tests on FOD flat specimens with different radii at the leading edges and then studied the effect of different leading-edge radii on the high-cycle fatigue strength of FOD blades. Witek, a scholar at the Rzeszow University of Science and Technology in Poland, used a shaker to directly perform high-cycle vibration fatigue test research on real blades and achieved good results. He used ABAQUS software to calculate the stress distribution during blade vibration. The results showed that the blades would generate high stress loads due to vibration under the first-order mode, and there was a high stress gradient in the blade's first-order nodal line cross-section [16]. Based on the research on high-cycle fatigue test or complete blade, Witek [17] prefabricated different shapes of notches on the leading edge of the PZL-10W engine compressor blade and conducted a high-cycle fatigue test to study the effect of the notch shape on the fatigue strength of the blade. When studying the cause of fatigue failure of a certain type of naval helicopter engine blade, Witek et al. [18] found that the corrosion pits at the blade leading edge caused by salt spray seriously endangered the HCF performance of blades, just like the defects at the blade leading edge caused by FOD. In order to improve the anti-FOD capability of engine blades, surface strengthening processes such as shot peening [19] and laser shock peening [20] have been performed to blades in recent years. The impact of these processes on the fatigue strength of FOD blades has also become focuses on FOD-related research.

Structural fatigue problems usually occur during the engineering application of metal components, especially in high stress concentration positions such as notches and welded joints [21, 22]. Based on the idea of structural elements, Neuber [23] proposed an average stress model to predict notched fatigue strength and gave a Neuber formula to calculate notched fatigue coefficients K_f. Peterson [24] proposed a simpler Peterson formula based on Neuber's research, which is widely used in engineering. Ruschau et al. [25] took the FOD damage made by an air cannon as a notch and predicted the HCF strength of the damaged TC4 specimen through the above-mentioned empirical formula of fatigue notch coefficient. It was found that the predicted values were higher than experimental results. Based on the research by Neuber and Peterson, Taylor [26] developed a method called the Theory of Critical Distance (TCD), which took the average stress of stresses within a certain area around the root cross-section of the notch as the effective stress to predict the fatigue limit. Hudak et al. [27] proposed a Worst Case Notch (WCN) model for HCF strength prediction for damaged parts. This model assumes that microcracks generate at the root of damage since the initial fatigue loading stage; thus, the HCF fatigue strength of damaged parts could be predicted by the boundary conditions of crack propagation. The boundary conditions of crack propagation can be used to estimate the HCF strength. Nowell et al. [28] applied a short crack arrest model which is similar to the WCN model to predict the HCF strength of three different-sized FOD notches. The prediction result is significantly lower than the experimental value. They believes that the main factor affecting the prediction accuracy is that the model does not consider the effect of compressive residual stress at the damage root on the crack propagation boundary. Chaves et al. [29] proposed a method of fatigue limit prediction through stress gradient and linear elastic analysis under remote loading based on the microstructural fracture mechanics model (Navarro and De los Rios [30]). The prediction model was applied to circle holes and V-notches under I-mode loading. The results show that the prediction error is within 12% and the accuracy is high.

This paper focuses on the effect of FOD on the HCF limit of a 1Cr11Ni2W2MoV stainless steel flat plate specimen, as well as on the prediction method for the HCF limit. Through FOD and HCF tests, the influences of damage parameters on the notch fatigue limit were analysed, and the microcharacteristics of notch and fracture were observed. Both the average stress model and the WCN model were used to predict the fatigue limit of FOD notch, and the high accuracy range of the WCN model was given after the research.

2. Experimental Investigations

2.1. FOD Test

2.1.1. Specimen Details. 1Cr11Ni2W2MoV is a kind of multi-element alloying martensitic stainless steel, which is used after quenching and tempering. The process plasticity and welding performance of 1Cr11Ni2W2MoV are great. It can be manufactured to die forgings with complex shapes and welded structures. It is suitable for manufacturing shaft, disk, blade, compression spring, and other components working under 550°C and in a high humidity environment. Material properties of 1Cr11Ni2W2MoV at room temperature are shown in Table 1.

A flat plate specimen is designed for the FOD test. The size of the specimen is shown in Figure 1.

The foreign objects used in the FOD test are GCr15 steel balls with diameters of 2 mm, 3 mm, and 4 mm, respectively, which are fixed by a cylindrical nylon sabot. Material properties of GCr15 at room temperature are shown in Table 1.

2.1.2. Device Details. FOD tests on flat plate specimens were carried out by an air cannon system to obtain damages more consistent with features of that in real service. The test system consists of a gas cylinder, a gas storage tank, a loading mechanism, a pressure sensor, a target chamber, solenoid valves, and other components. The picture of the air cannon system is shown in Figure 2.

After the FOD test, a HIROX KH-7700 three-dimensional stereomicroscope was used to observe the macrofeatures of the damage notch, whose minimum resolution is 1 μm.

2.1.3. Test Method. The impact speed was 290 m/s in the test, with an incident angle of 0°. The impact diagram is shown in Figure 3.

2.2. Fatigue Test

2.2.1. Specimen Details. The HCF test specimens are divided into the smooth rectangular section specimen and notched specimen. The smooth rectangular section specimen designed according to GB3075-82 (a Chinese national standard for metal axial fatigue test) [31] is shown in Figure 4 and used to obtain the fatigue limit of 1Cr11Ni2W2MoV at stress ratio $R = 0.8$ (working stress ratio of aeroengine at cruise state). The notched specimen is a flat plate sample after the FOD test in Section 2.1. In fact, the residual stress at the notch root caused by FOD will affect the stress ratio, which cannot be maintained at 0.8. However, considering the complexity of quantitative analysis on and the inconvenience of measurement on residual stress in engineering application, in-depth research on this point is not conducted in the paper. Thus, all tests are carried out with the stress ratio $R = 0.8$.

2.2.2. Device Details. The HCF tests on both smooth rectangular section specimens and notched specimens were carried out by QBQ-100 a high-frequency fatigue testing machine.

2.2.3. Test Method. The step-loading method (Maxwell and Nicholas [32]) was used to perform HCF tests to obtain the HCF limit of each smooth rectangular section specimen and notched specimen at the life of 10^7 cycles.

Table 1: Material properties of 1Cr11Ni2W2MoV and GCr15 at room temperature.

Material	Density ρ (kg/m^3)	Elastic modulus E (GPa)	Poisson's ratio μ
1Cr11Ni2W2MoV	7800	198	0.301
GCr15	7850	210	0.300

The method is described as follows. If the specimen survived the initial step of loading, the stress level would be increased by 10% and the test repeated. This would continue until the specimen failed in less than 10^7 cycles. If we assume that the fatigue damage accumulates linearly in the last step of loading, the fatigue limit for the life of 10^7 cycles could be calculated by the following formula:

$$\sigma_e = \sigma_{\mathrm{pr}} + \frac{N_f}{10^7} \cdot \left(\sigma_f - \sigma_{\mathrm{pr}}\right), \tag{1}$$

where σ_e is the fatigue limit at 10^7 cycles, σ_{pr} is the maximum stress level of the previous stress step, N_f is the number of cycles when the last stress step fails, and σ_f is the maximum stress level of the last stress step.

The load spectrum of the notched specimen is shown in Figure 5.

2.3. SEM Observation. The microcharacteristics of FOD notches and fatigue fractures of specimens were observed by JSM-7001 SEM. The main characteristics of FOD notches include loss of material (LOM), lamellar structure, and microcrack, and the main characteristics of fatigue fractures include the fatigue source area and crack growth area.

The device parameters are as follows:

(i) Resolution: 1.4 nm

(ii) Acceleration voltage: 30 kV

(iii) Magnification: 40x~20000x

2.4. Crack Growth Test

2.4.1. Specimen Details. The crack growth test specimen is a compact tensile sample. The shape and size of the sample are designed according to relevant requirements in GB/T6398 (a Chinese national standard for fatigue crack growth rate test) [33], and then, the sample is processed by wire cutting before the test. The designing size of the crack growth test specimen is shown in Figure 6. The crack growth direction is perpendicular to the rolling direction.

2.4.2. Device Details. The tests were carried out by the 809 axial/torsional test system (MTS), and the crack length was measured by a Crack Opening Displacement (COD) gauge, as shown in Figure 7. Before the crack growth test, the pre-cracking test [34, 35] was carried out and the length of pre-cracking is 1.7 mm. The controlled stress ratio during the

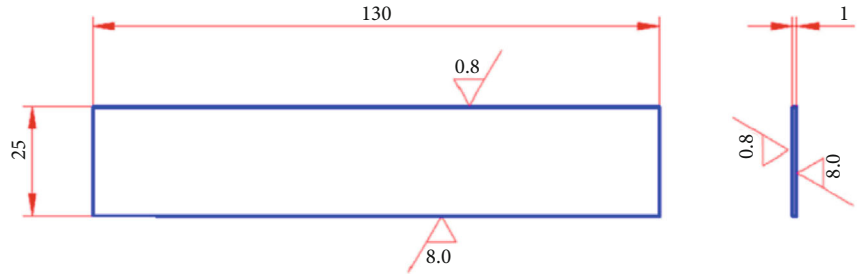

Figure 1: Size of flat plate specimen.

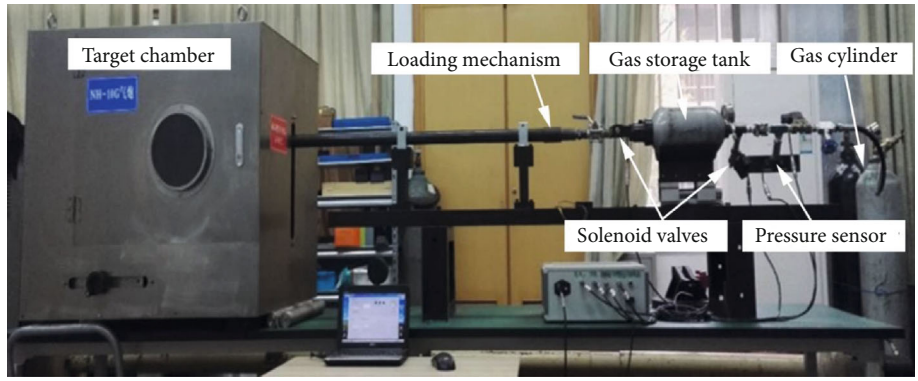

Figure 2: Air cannon system.

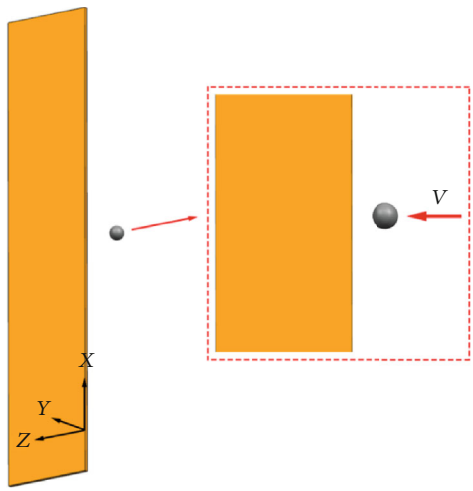

Figure 3: Impact diagram.

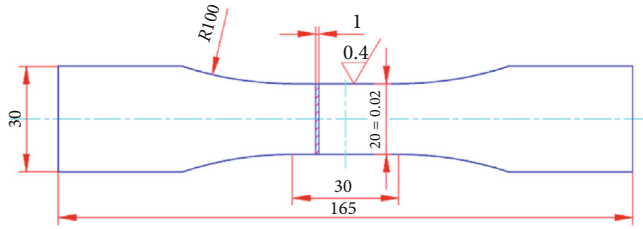

Figure 4: Designing parameters of smooth rectangular section specimen.

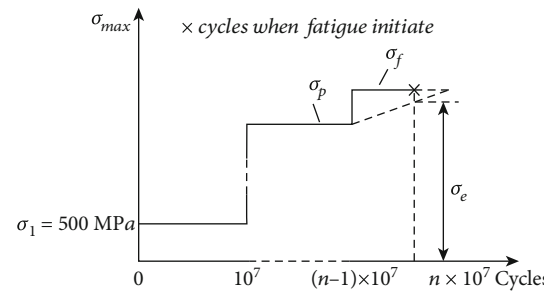

Figure 5: Load spectrum for HCF test.

test is 0.8, the frequency of precracking is 8 Hz, and the frequency of crack growth is 10 Hz. When the crack length reaches about 36 mm, the test is terminated.

2.4.3. Test Method. The K gradient method controlled by constant force was used in the test. During the test, the gradient value C of stress intensity factor K is constant, and the calculation method of stress intensity factor range ΔK is given by the following formula. The compliance method was used to measure the crack length:

$$\Delta K = \frac{\Delta P}{B\sqrt{W}} \times \frac{(2+a)}{(1-\alpha)^{3/2}}\left(0.886 + 4.64\alpha - 13.32\alpha^2 + 14.72\alpha^3 - 5.6\alpha^4\right), \quad (2)$$

where $\alpha = a/W$, ΔP is the range of load, a is the calculated crack length, B is the thickness of the specimen, and W is the width of the specimen.

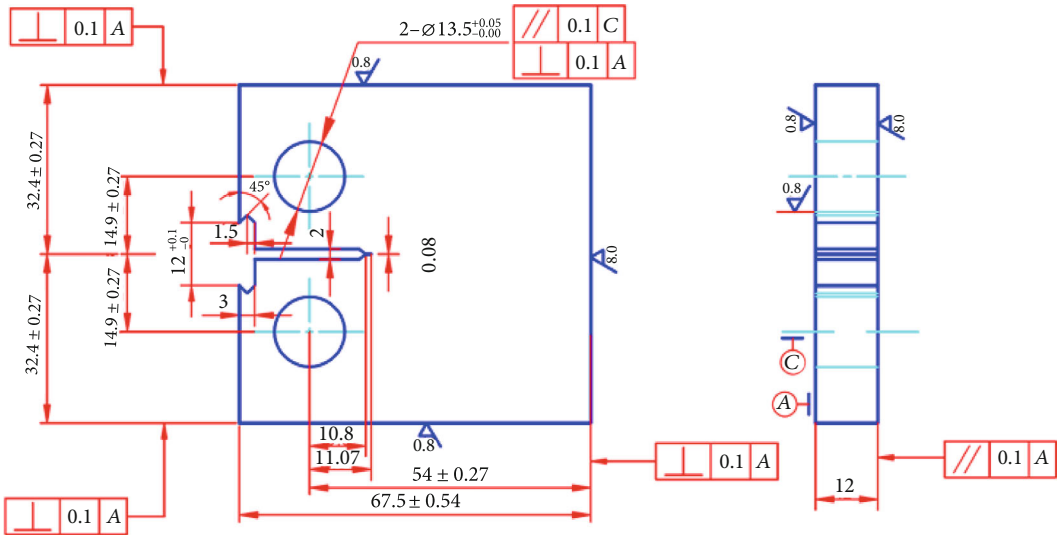

Figure 6: Designing size of the crack growth test specimen.

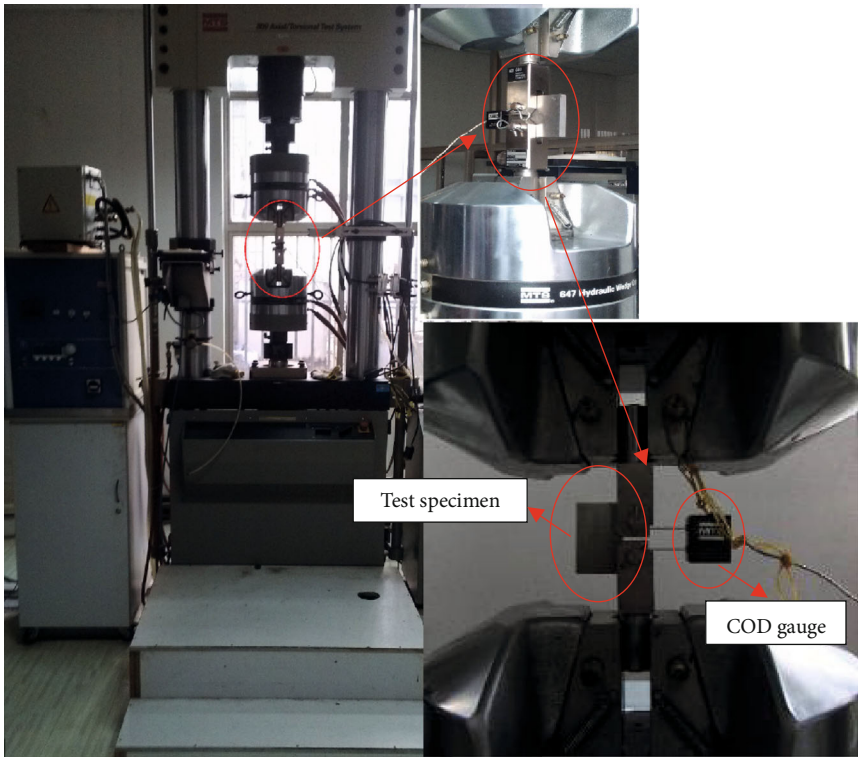

Figure 7: 809 axial/torsional test system and COD gauge.

During the steady-state crack growth stage, the relationship between the crack growth rate da/dN and stress intensity factor amplitude ΔK can be described by the Paris power function:

$$\frac{da}{dN} = C\Delta K^n. \tag{3}$$

Take logarithm operation on both sides of the above formula,

$$\lg\left(\frac{da}{dN}\right) = \lg C + n \lg \Delta K. \tag{4}$$

Generally, at least 5 pairs of $(da/dN)_i$ and corresponding $(\Delta K)_i$ which satisfy 10^{-7} mm/cycle $\leq da/dN \leq 10^{-6}$ mm/

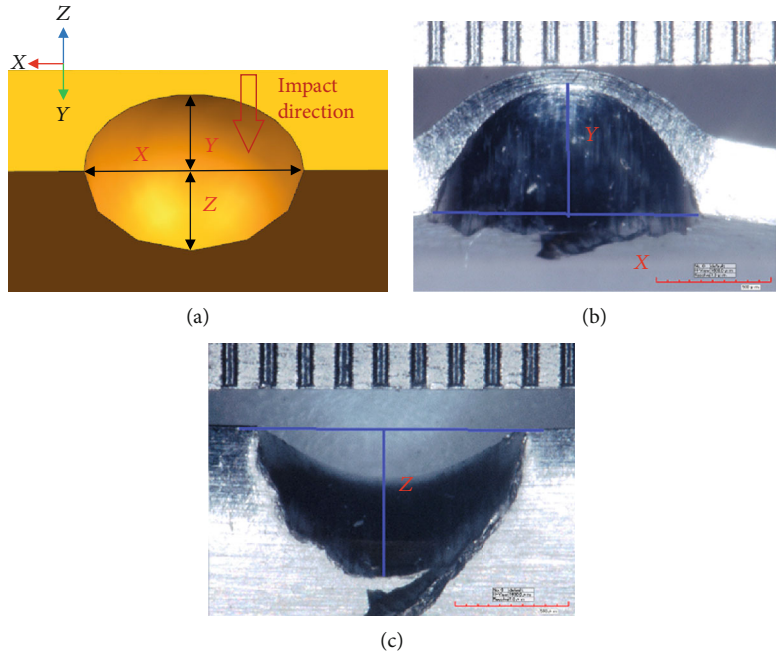

Figure 8: Damage size definition: (a) 3D sketch of the notch; (b) damage width X and damage thickness Y; (c) damage depth Z.

cycle should be taken as the threshold value for fatigue crack calculation [35]. lg (da/dN) in formula (4) is taken as the independent variable for the matching of lg (da/dN) – lg (ΔK) data points by the linear regression method. The fatigue crack growth threshold ΔK_{th} is ΔK corresponding to $da/dN = 10^{-7}$ mm/cycle according to the matching results.

3. Results and Discussion

3.1. FOD Test Results

3.1.1. FOD Size. FOD tests were conducted on 13 flat plate specimens. The maximum damage size along the length direction of the specimen is defined as the damage width X, the maximum damage size along the thickness direction of the specimen is defined as the damage thickness Y, and the maximum damage size along the width direction of the specimen is defined as the damage depth Z. The definition of damage sizes is shown in Figure 8.

The FOD test results of flat plate specimens are shown in Table 2. The relationship between damage size and steel ball diameter is shown in Figure 9, where the straight line formed by blue stars represents the mean value of damage size. It can be found from Figure 9 that the width X, thickness Y, and depth Z of the damage notch all increase with the diameter of the steel ball. The damage width X and depth Z are relatively stable with the same diameter of the impact steel ball, while damage thickness Y shows great fluctuation due to the deviation of impacting position in the thickness direction.

3.1.2. Microscopic Features of Notches. The damage notches on No. 7 samples were observed by SEM, and their microscopic characteristics are shown in Figure 10. It can be seen from the figure that there is a relatively smooth extrusion area at the root of the notch formed by the high-speed impact of the steel ball, and there is obvious plastic deformation accompanied by loss of material (LOM) on the side of the notch. If further amplified by the notch root area, it can be found that there are lamellar structures forming at the side of the notch due to the shear stress in the impacting process, accompanying with microcracks. These microdamage characteristics provide favourable conditions for the initiation and propagation of fatigue cracks and reduce the fatigue performances of materials at the notch.

Table 2: HCF limit of notched specimens.

No.	Diameter (mm)	X (mm)	Y (mm)	Z (mm)	σ_t (MPa)
1	2	1.69	0.96	0.43	615
2	2	1.66	0.79	0.5	776
3	3	2.77	1.34	0.82	667
4	3	2.5	1.31	0.99	658
5	3	2.87	1.56	1.04	637
6	3	2.65	1.21	1.26	610
7	3	2.52	0.96	1.11	761
8	3	2.77	1.34	1.39	599
9	3	2.54	1.19	1.49	600
10	3	2.57	1.11	1.22	814
11	4	3.54	1.69	1.94	507
12	4	2.85	1.06	1.61	607
13	4	3.41	1.6	1.56	567

σ_t: HCF limit.

3.2. Fatigue Test Results

3.2.1. Fatigue Limit. The fatigue limit results of smooth rectangular section specimens at the life of 10^7 cycles with stress ratio 0.8 are shown in Table 3.

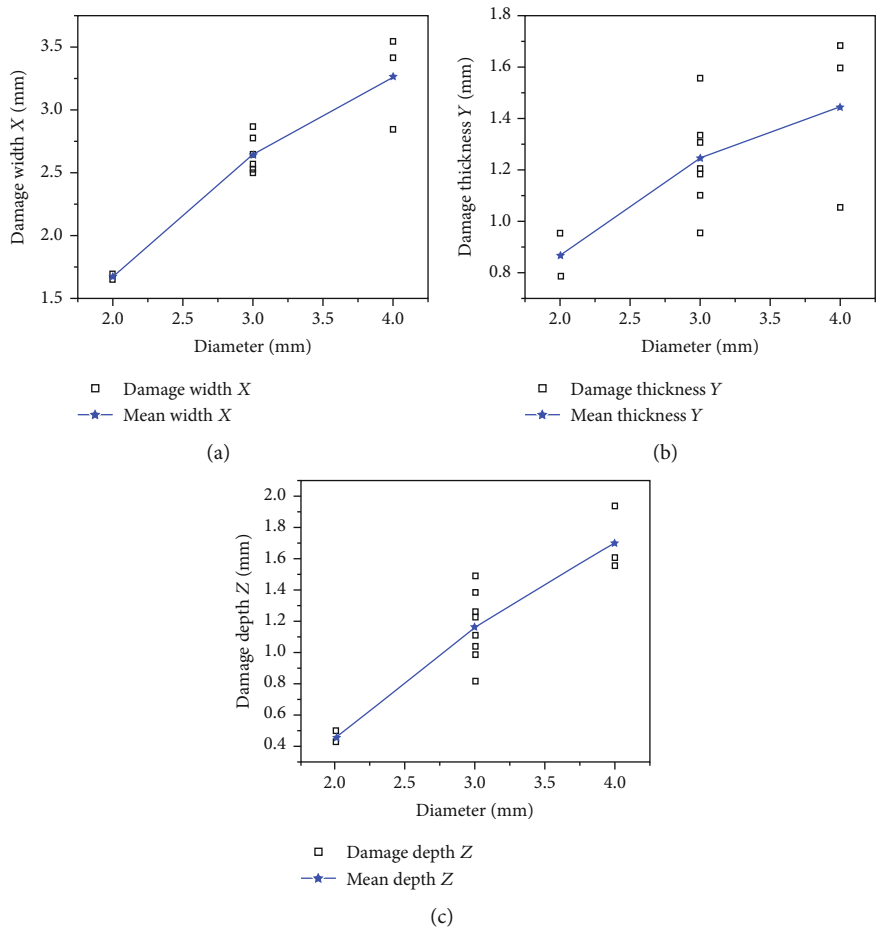

Figure 9: The relationship curve between damage size and steel ball diameter: (a) damage width X with steel ball diameter; (b) damage thickness Y with steel ball diameter; (c) damage depth Z with steel ball diameter.

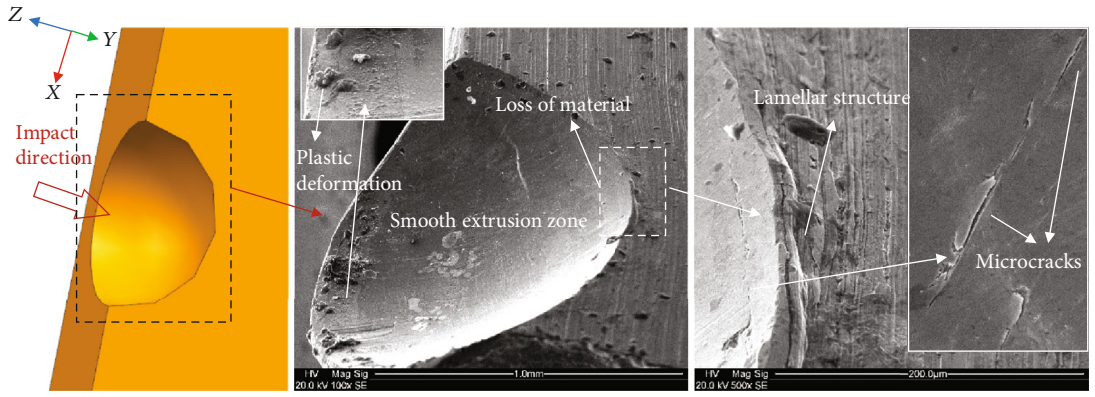

Figure 10: The microscopic features of FOD notch on the No. 7 flat plate specimen.

Table 3: HCF limit of smooth rectangular section specimens.

No.	σ_t (MPa)	Mean value (MPa)
B-1	950.5	
B-2	949	949.83
B-4	950	

The fatigue limit results of 13 notched specimens at the life of 10^7 cycles with stress ratio 0.8 are shown in Table 2.

The relationship between the HCF limit of FOD flat plate specimens and FOD parameters is shown in Figure 10 and the parameters including damage width X, damage depth Z, and steel ball diameter.

Figures 11(a) and 11(b) show the relationship between the HCF limit and damage size, in which the red line is the

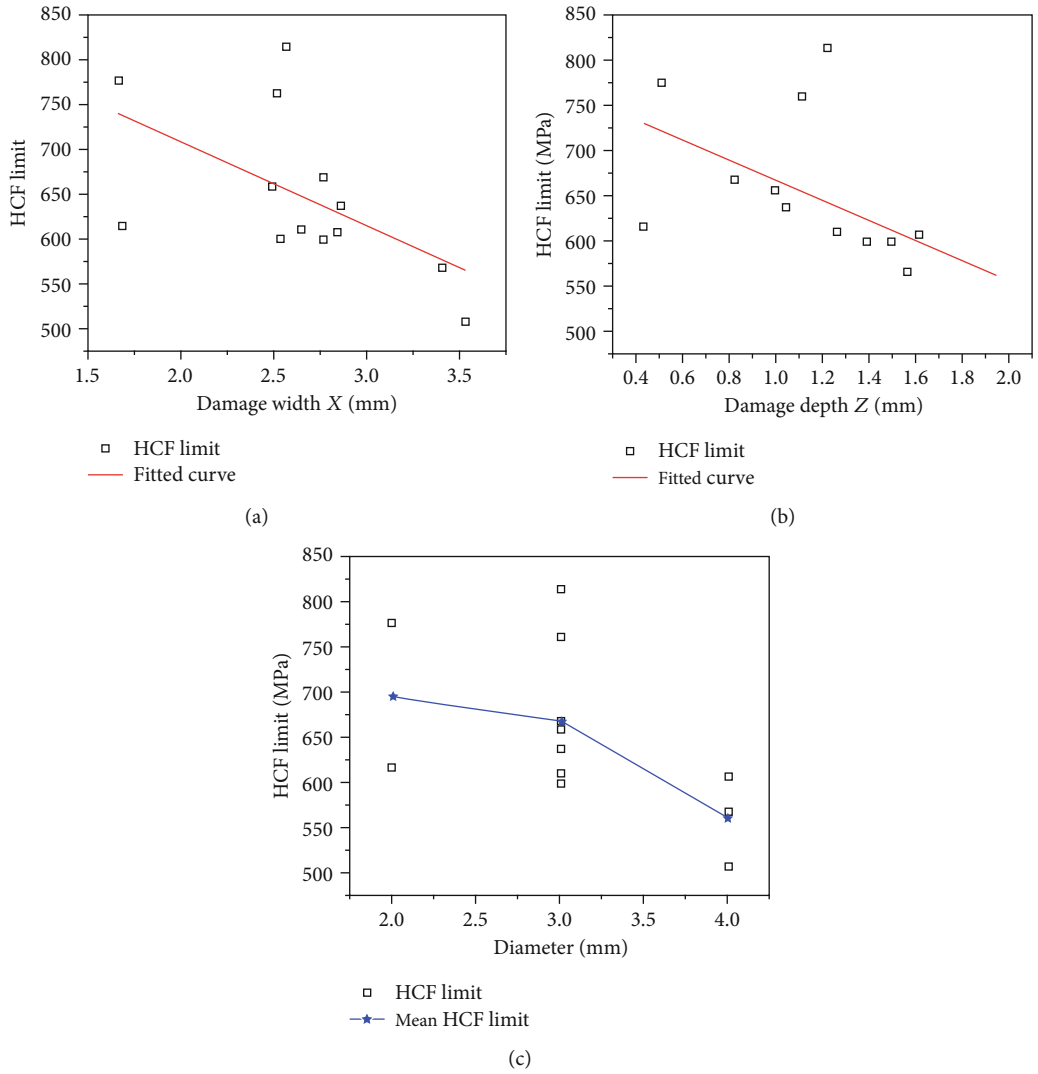

Figure 11: The relationship between HCF limit and FOD parameters: (a) HCF limit with damage width X; (b) HCF limit with damage depth Z; (c) HCF limit with steel ball diameter.

fitting curve of the HCF limit. It is obvious that the HCF limit decreases with the increase of damage depth Z and damage width X. However, the dispersion of damage width X and HCF limit is larger than that of damage depth Z. It shows that the effect of notch depth on HCF is larger than that of notch width.

The relationship between the HCF limit and steel ball diameter is shown in Figure 11(c), in which the straight line formed by blue stars represents the mean value of the HCF limit. It can be seen that the HCF limit decreases with the increase of steel ball diameter, which is consistent with the relationship between damage depth Z and steel ball diameter shown in Figure 9(c). The HCF limit under the same steel ball diameter has certain dispersion, which is caused by the characteristics of the air cannon system.

3.2.2. Fracture Microscopic Features. The fatigue fractures on No. 9 notched specimens were observed and analysed by SEM, as shown in Figure 12. It can be seen from the figure that the fatigue fracture occurs at the root surface of the FOD notch. There are two fatigue source zones, Zones A and B in Figure 11(a), which are located on both sides of the thickness direction of the flat plate specimen and near the notch tip. The fatigue source zone usually occurs at the notch tip where the notch root surface meets the specimen surface. The crack initiation becomes flat and fine since it is torn open and extruded repeatedly by HCF loads. The fracture surface can be distinguished from the fatigue source area (dark) and the crack growth area (light). The darker colour of the fatigue source area is due to the long exposure time in the air and the oxidation of the material after the crack initiation. The red arrow in Figure 12(a) indicates the incident direction of the steel ball. Zone A and Zone B are the locations of the fatigue source area. Since the crack started at different heights during the initiation process, it would meet each other in the propagation process, and then, a river pattern came out converging to the fatigue source (Figure 12(b)). The adiabatic shear band (ASB) can be observed near the notch root surface in Zone C, caused by steel ball impact [36]. What is more, loss of material (LOM) and plastic deformation can be

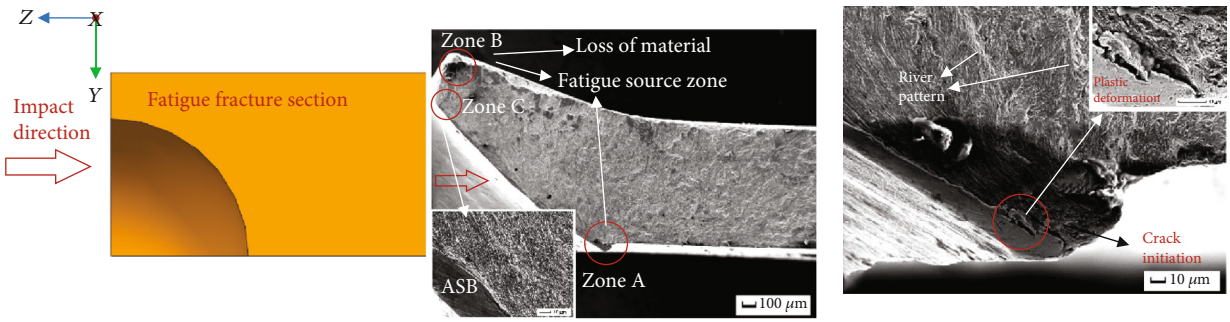

Figure 12: The microscopic features of fatigue fracture on No. 9 flat plate specimen: (a) global view; (b) Zone A.

observed in the fatigue source area, indicating that FOD provides favourable conditions for the initiation of fatigue cracks. Under the action of the fatigue load, the fatigue crack gets rapid growth and finally causes the specimen fracture failure.

3.3. Crack Growth Test Results. The crack growth rate measured by the crack growth test is shown in Figure 13, from which the crack growth threshold of 1Cr11Ni2W2MoV can be calculated as 6.23 MPa$\sqrt{\text{m}}$ when the stress ratio $R = 0.8$.

3.4. Fatigue Limit Prediction. The stress concentration caused by the notch has a significant effect on the fatigue performance of the components. The theoretical stress concentration factor K_t is based on the assumption that the material is elastic, and it only depends on the geometry of the component. However, in engineering practice, there is plastic deformation in varying degrees of the notch. Therefore, it is necessary to use the fatigue notch factor K_f to characterize the fatigue strength of notched components.

The fatigue notch factor K_f is defined as the ratio between the fatigue limit of the smooth rectangular section specimen and the fatigue limit of the notched specimen under the same conditions and cycles. The formula is as follows:

$$K_f = \frac{\sigma_{\text{smooth}}}{\sigma_{\text{notched}}}, \tag{5}$$

where $\sigma_{\text{smooth}} = 949.83$ MPa, as shown in Table 3.

3.5. Prediction Model for FOD Specimen Fatigue Limit Based on Peterson Formula. On the basis of Neuber's research [23], Peterson assumed that stress decreases linearly from the notch root inward. When the average stress within a certain distance from the notch root is greater than or equal to the fatigue limit of the smooth specimen, the fatigue failure will occur. The Peterson formula is as follows:

$$K_f = 1 + \frac{K_t - 1}{1 + a_p/\rho}, \tag{6}$$

where ρ is the radius of the notch root, which is approximately equal to the radius of the steel ball in this paper. a_p is the material constant under the influence of tensile stress

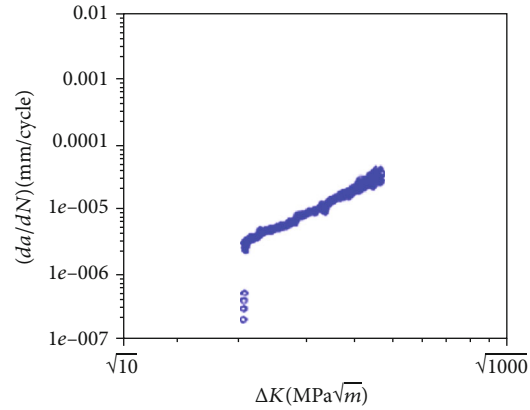

Figure 13: Crack growth rate of 1Cr11Ni2W2MoV ($R = 0.8$).

value, which could be determined by the empirical formula $a_p = (270/\sigma_b)^{1.8}$. σ_b is tensile strength of 1Cr11Ni2W2MoV, which equals to 955 MPa.

For sharp notches, the following equation can be used to calculate K_t [37]:

$$Kt\left(\frac{\rho}{d}\right) = \left(\frac{1 + 2d}{\rho}\right) f\left(\frac{\rho}{d}\right), \tag{7}$$

where d is the depth of the notch, ρ is the radius of the notch root, and $f(\rho/d)$ is given by the following equation:

$$f\left(\frac{\rho}{d}\right) \cong 1 + 0.122\left(\frac{1}{1 + \rho/d}\right)^{5/2}. \tag{8}$$

The theoretical stress concentration factor K_t can be calculated according to formula (7), and the prediction fatigue notch factor K_f can be calculated according to formula (6). The fatigue limit of the notched specimen can be predicted according to formula (6). The calculation results and error analysis are listed in Table 4.

The error distribution on the fatigue limit of FOD flat plate specimens predicted by the Peterson formula is shown in Figure 14, and the error is defined by the following formula. It can be seen from the figure that the prediction error lies within the range of (-55%, -30%), except one 13.7%.

Table 4: Fatigue limit predictions by Peterson formula and WCN model.

No.	Diameter (mm)	Z (mm)	K_t	K_f	σ_P (MPa)	ΔS_e	σ_W (MPa)	σ_{test} (MPa)	ErrorP	ErrorW
1	2	0.43	1.87	1.79	530.76	130.31	651.54	615	-13.70%	5.94%
2	2	0.5	2.02	1.92	494.58	122.07	610.37	776	-36.27%	-21.34%
3	3	0.82	2.11	2.04	465.50	98.12	490.61	667	-30.21%	-26.45%
4	3	0.99	2.35	2.26	420.06	90.15	450.74	658	-36.16%	-31.50%
5	3	1.04	2.42	2.33	408.29	88.16	440.80	637	-35.90%	-30.80%
6	3	1.26	2.73	2.62	363.27	80.79	403.95	610	-40.45%	-33.78%
7	3	1.11	2.52	2.42	392.84	85.59	427.97	761	-48.38%	-43.76%
8	3	1.39	2.91	2.79	340.93	77.24	386.19	599	-43.08%	-35.53%
9	3	1.49	3.05	2.92	325.48	74.81	374.06	600	-45.75%	-37.66%
10	3	1.22	2.67	2.56	370.72	81.99	409.94	814	-54.46%	-49.64%
11	4	1.94	3.00	2.90	327.25	66.22	331.08	507	-35.45%	-34.70%
12	4	1.61	2.65	2.57	369.45	72.19	360.94	607	-39.13%	-40.54%
13	4	1.56	2.60	2.52	376.78	73.25	366.23	567	-33.55%	-35.41%

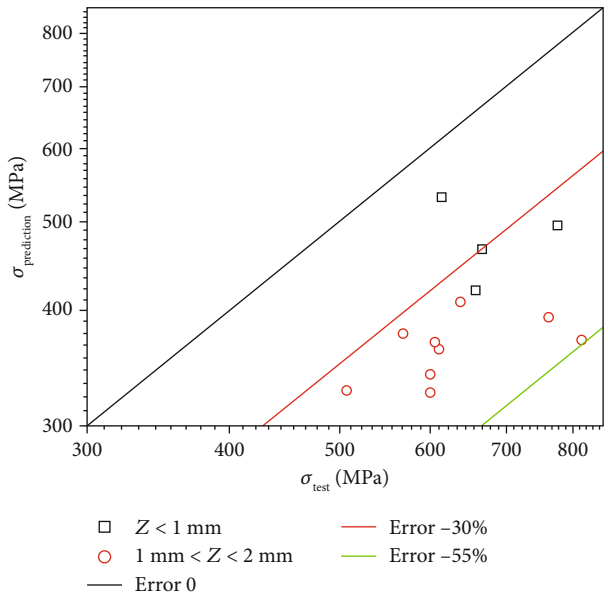

Figure 14: Prediction error distribution of Peterson formula.

Prediction values for all FOD flat plate specimens are lower than test values, which is considered conservative:

$$\text{error} = \frac{\left(\sigma_{\text{prediction}} - \sigma_{\text{test}}\right)}{\sigma_{\text{test}}}. \tag{9}$$

3.6. Prediction Model for FOD Specimen Fatigue Limit Based on WCN Model. Microcracks and corresponding cracks which do not propagate along the stress gradient direction of the notch could be regarded as the WCN model [27]. The WCN model takes the nominal stress threshold as a function of elastic stress concentration factor K_t and crack size a. The nominal stress threshold decreases with the increase of K_t and notch sensitivity. However, the nominal stress threshold does not decrease with the increase of K_t when the predicted K_t (by the WCN model) exceeds the limit value. It is mainly caused by the generation of end crack and nonpropagating crack. For the notch with fixed depth and different root radii, the nominal stress threshold increases with radius, and there is a limit radius. When the radius exceeds the limit radius, the crack will not propagate.

The aim of the WCN model is to quantify the correlation among notch depth, root radius, stress concentration factor, and other parameters, so as to solve the problem of the notch fatigue limit in a systematic way. Because of the great amount of microdamages in the notch caused by FOD and the fatigue cracks initiated at the microcrack or micronotch, the WCN model is selected to predict the fatigue limit of the notched flat plate specimen.

Generally speaking, the stress threshold is a function of the FOD notch size, the loading mode, and the material parameters. In this paper, the crack propagation threshold of 1Cr11Ni2W2MoV is obtained by the crack growth test.

The formula of the WCN model is

$$\Delta S_e = \frac{\Delta K_{\text{th}}}{F\sqrt{\pi}\left(\sqrt{a_0} + \sqrt{d}\right)}, \tag{10}$$

$$a_0 = \frac{1}{\pi}\left(\frac{\Delta K_{\text{th}}}{F\Delta\sigma_e}\right)^2, \tag{11}$$

where ΔS_e is stress amplitude at the root of the notch, a_0 is small crack parameters, ΔK_{th} is the crack propagation threshold (obtained from the crack growth test result in Section 3.3), F is the finite-thickness correction function (if the crack depth is much smaller than its length, F is about 1.12, and most cases of FOD are those where cracks are small [37]), and $\Delta\sigma_e$ is the fatigue limit of the smooth specimen at 10^7 cycles.

Small crack parameters a_0 can be calculated by formula (11), and the stress amplitude ΔS_e can be calculated by formula (10). According to the relationship between stress amplitude ΔS_e and stress ratio R, the prediction value of the

HCF limit of the notch root can be calculated. The prediction results are shown in Table 4, and the error distribution graph is shown in Figure 15. It can be seen from the figure that the prediction error lies within the range of (-50%, 6%). Most prediction values of FOD flat plate specimens are lower than test values, which is considered conservative, just like the prediction results by the Peterson formula.

3.7. Comparison. It can be seen from Figure 16 and Table 4 that the fatigue limit predicted by the Peterson formula and WCN model is both conservative, and almost all prediction error of the Peterson formula is between (-55%, -30%), while that of the WCN model is between (-50%, 20%). For the notch with damage depth Z greater than 1 mm, the predictions by the Peterson formula and WCN model are similar, and the errors are all more than 30%. The predictions by the WCN model are slightly accurate. For the notch with damage depth Z less than 1 mm, the prediction accuracy of the WCN model is higher than that of the Peterson formula, and the error lies within 32%. The results show that the WCN model is more accurate for the HCF limit prediction for specimens with small damage depth (<1 mm).

The possible reasons for the prediction error are as follows. The Peterson formula is based on the point stress model. It is assumed in the Peterson formula that there is only uniaxial stress at the notch of the specimen, without considering the strengthening effect, three-dimensional stress concentration, loading conditions, and complex microdamage characteristics at the notch. Therefore, the prediction results are conservative. In the WCN model, when the notch size is small, the parameter notch depth d in formula (10) is accurate. However, when the notch size is large, the parameter is not accurate enough, so it is necessary to research the model expression more deeply.

4. Conclusions

FOD tests, HCF tests, and crack growth tests under stress ratio $R = 0.8$ were carried out for 1Cr11Ni2W2MoV stainless steel specimens. The Peterson formula and WCN model were used to predict the HCF limit of notched specimens. The results obtained in this study allow us to draw the following conclusions:

(1) FOD notch sizes (damage width X, damage thickness Y, and damage depth Z) increase with the steel ball diameter, and the damage thickness Y shows great fluctuation

(2) The high-speed impact of the steel ball results in a smooth extrusion area at the notch root, accompanying plastic deformation, loss of material, and microcracks at the side of the notch. These microdamage characteristics promote the initiation and propagation of fatigue cracks. Therefore, fatigue fracture occurs at the root of the FOD notch, which displays a dark fatigue source area

(3) The HCF limit of FOD flat plate specimens was predicted by the Peterson formula and WCN model. The predictions by the Peterson formula are conservative, and the error lies within (-55%, -30%), except one 13.7%. The predictions by the WCN model are more accurate, especially for the damage depth $Z < 1$ mm (errors less than 32%). The prediction errors of the notch fatigue limit for damage depth $Z > 1$ mm are more than 30%, but most of them are still better than the predictions by the Peterson formula

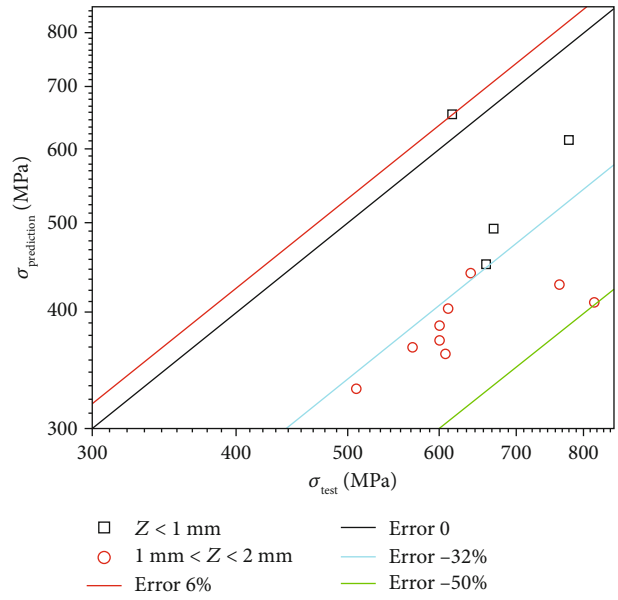

Figure 15: Prediction error distribution of the WCN model.

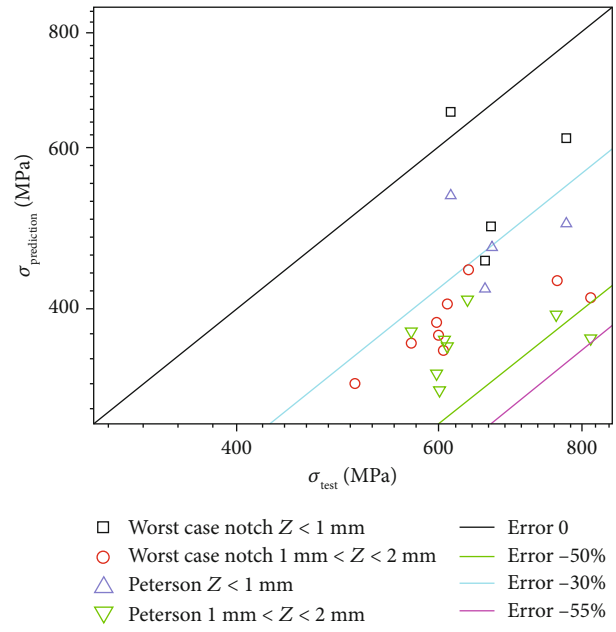

Figure 16: Prediction error distribution of WCN model and Peterson formula.

Z: damage depth; K_t: calculation stress concentration factor; K_f: predicted notch fatigue factor; σ_P: HCF limit

predicted by Peterson formula; ΔS_e: stress amplitude at the root of notch; σ_W: HCF limit predicted by WCN model; σ_{test}: HCF limit tested by HCF test; ErrorP: prediction error of Peterson formula; ErrorW: prediction error of WCN model.

Data Availability

The test data used to support the findings of this study are included within the article.

Additional Points

Highlights. (i) FOD notch size (damage width X, damage thickness Y, and damage depth Z) increases with the increase of steel ball diameter. (ii) The high-speed impact of the steel ball results in the smooth extrusion area at the notch root, accompanying plastic deformation, loss of material, and microcracks at the side of the notch. (iii) The prediction results of the Peterson formula are conservative, and the error range is (-55%, -30%). (iv) The prediction results of "Worst Case Notch" model are more accurate, especially for the damage depth $Z < 1$ mm, whose errors are within 32%.

Conflicts of Interest

The authors declare that they have no conflicts of interest.

Acknowledgments

This work was supported by a Project supported by the National Natural Science Foundation of China (Grant No. 51301090).

References

[1] Y. Zhou, Y. Sun, and W. Cai, "Bird-striking damage of rotating laminates using SPH-CDM method," *Aerospace Science and Technology*, vol. 84, pp. 265–272, 2019.

[2] J. Pernas-Sánchez, J. A. Artero-Guerrero, D. Varas, and J. López-Puente, "Analysis of ice impact process at high velocity," *Experimental Mechanics*, vol. 55, no. 9, pp. 1669–1679, 2015.

[3] S. Mall, J. L. Hamrick II, and T. Nicholas, "High cycle fatigue behavior of Ti–6Al–4V with simulated foreign object damage," *Mechanics of Materials*, vol. 33, no. 11, pp. 679–692, 2001.

[4] B. A. Cowles, "High cycle fatigue in aircraft gas turbines—an industry perspective," *International Journal of Fracture*, vol. 80, no. 2-3, pp. 147–163, 1996.

[5] G. Yupu, Z. Zhenhua, C. Wei, and G. Deping, "Foreign object damage to fan rotor blades of aeroengine part II: numerical simulation of bird impact," *Chinese Journal of Aeronautics*, vol. 21, no. 4, pp. 328–334, 2008.

[6] J. O. Peters, B. L. Boyce, A. W. Thompson, R. O. Ritchie, and O. Roder, "Role of foreign-object damage on thresholds for high-cycle fatigue in Ti-6Al-4V," *Metallurgical and Materials Transactions A: Physical Metallurgy and Materials Science*, vol. 31, no. 6, pp. 1571–1583, 2000.

[7] H. K. Farahani, M. Ketabchi, S. Zangeneh, and M. Hosseini, "Characterization of damage induced by impacting objects in udimet-500 alloy," *Journal of Failure Analysis and Prevention*, vol. 16, no. 4, pp. 629–634, 2016.

[8] M. R. Bache, C. Bradshaw, and W. Voice, "Characterisation of foreign object damage and fatigue strength in titanium based aerofoil alloys," *Materials Science and Engineering*, vol. 354, no. 1-2, pp. 199–206, 2003.

[9] S. Oakley and D. Nowell, "Prediction of the combined high- and low-cycle fatigue performance of gas turbine blades after foreign object damage," *International Journal of Fatigue*, vol. 29, no. 1, pp. 69–80, 2007.

[10] P. Duó, J. Liu, D. Dini, M. Golshan, and A. M. Korsunsky, "Evaluation and analysis of residual stresses due to foreign object damage," *Mechanics of Materials*, vol. 39, no. 3, pp. 199–211, 2007.

[11] X. Chen and W. J. Hutchinson, "Foreign object damage and fatigue crack threshold: cracking outside shallow indents," *International Journal of Fracture*, vol. 107, no. 1, pp. 31–51, 2001.

[12] S. M. Marandi, K. Rahmani, and M. Tajdari, "Foreign object damage on the leading edge of gas turbine blades," *Aerospace Science and Technology*, vol. 33, no. 1, pp. 65–75, 2014.

[13] X. Chen, "Foreign object damage on the leading edge of a thin blade," *Mechanics of Materials*, vol. 37, no. 4, pp. 447–457, 2005.

[14] J. J. Ruschau, T. Nicholas, and S. R. Thompson, "Influence of foreign object damage (FOD) on the fatigue life of simulated Ti-6Al-4V airfoils," *International Journal of Impact Engineering*, vol. 25, no. 3, pp. 233–250, 2001.

[15] C. M. Martinez, D. Eylon, and T. Nicholas, "Effects of ballistic impact damage on fatigue crack initiation in Ti–6A1–4v simulated engine blades," *Materials Science and Engineering: A*, vol. 325, pp. 465–477, 2002.

[16] L. Witek, "Crack propagation analysis of mechanically damaged compressor blades subjected to high cycle fatigue," *Engineering Failure Analysis*, vol. 18, no. 4, pp. 1223–1232, 2011.

[17] L. Witek, "Experimental crack propagation and failure analysis of the first stage compressor blade subjected to vibration," *Engineering Failure Analysis*, vol. 16, no. 7, pp. 2163–2170, 2009.

[18] L. Witek, M. Wierzbińska, and A. Poznańska, "Fracture analysis of compressor blade of a helicopter engine," *Engineering Failure Analysis*, vol. 16, no. 5, pp. 1616–1622, 2009.

[19] M. Frija, T. Hassine, R. Fathallah, C. Bouraoui, and A. Dogui, "Finite element modelling of shot peening process: prediction of the compressive residual stresses, the plastic deformations and the surface integrity," *Materials Science and Engineering: A*, vol. 426, no. 1-2, pp. 173–180, 2006.

[20] B. Lin, S. Zabeen, J. Tong, M. Preuss, and P. J. Withers, "Residual stresses due to foreign object damage in laser-shock peened aerofoils: simulation and measurement," *Mechanics of Materials*, vol. 82, pp. 78–90, 2015.

[21] A. Sapora, P. Cornetti, A. Campagnolo, and G. Meneghetti, "Fatigue limit: crack and notch sensitivity by finite fracture mechanics," *Theoretical and Applied Fracture Mechanics*, vol. 105, p. 102407, 2020.

[22] C. J. Wei and H. T. Kang, "Fatigue life prediction of spot-welded joints with a notch stress approach," *Theoretical and Applied Fracture Mechanics*, vol. 106, p. 102491, 2020.

[23] H. Neuber, "Theory of Notch Stresses," in *Kerbspannungslehre*, Springer, Berlin, 2nd edition, 1958.

[24] W. D. Pilkey, *Peterson's Stress Concentration Factors*, Wiley, America, 2nd edition, 2007.

[25] J. Ruschau, S. R. Thompson, and T. Nicholas, "High cycle fatigue limit stresses for airfoils subjected to foreign object damage," *International Journal of Fatigue*, vol. 25, no. 9-11, pp. 955–962, 2003.

[26] D. Taylor, *The Theory of Critical Distances: A New Perspective in Fracture Mechanics*, Elsevier, Netherlands, 1st edition, 2007.

[27] S. J. Hudak, K. S. Chan, G. G. Chell, Y. D. Lee, and M. C. RC, "A damage tolerance approach for predicting the threshold stresses for high cycle fatigue in the presence of supplemental damage," in *Fatigue*, L. David, S. Davidson, K. S. Chan, P. K. Liaw, R. S. Bellows, T. C. Zogas, and W. O. Soboyejo, Eds., pp. 107–120, TMS Annual Meeting 2002, Warrendale, 2002.

[28] D. Nowell, P. Duó, and I. F. Stewart, "Prediction of fatigue performance in gas turbine blades after foreign object damage," *International Journal of Fatigue*, vol. 25, no. 9-11, pp. 963–969, 2003.

[29] V. Chaves, C. Madrigal, and A. Navarro, "Fatigue limit predictions at stress concentrations using FEA and microstructural fracture mechanics," *Theoretical and Applied Fracture Mechanics*, vol. 87, pp. 11–20, 2017.

[30] A. Navarro and E. R. De los Rios, "An alternative model of the blocking of dislocations at grain boundaries," *Philosophical Magazine A*, vol. 57, no. 1, pp. 37–42, 1988.

[31] GB3075-82, *Metal axial fatigue test method*, Administration of quality supervision of the people's Republic of China, Beijing, 1982.

[32] D. C. Maxwell and T. Nicholas, "A rapid method for generation of a Haigh diagram for high cycle fatigue," in *Fatigue and Fracture Mechanics: 29th Volume*, T. Panontin and S. Sheppard, Eds., vol. 29, pp. 626–641, ASTM International, West Conshohocken, PA, 1999.

[33] GB/T6398-2000, "Test method for fatigue crack growth rate of metallic materials," Administration of quality supervision of the people's Republic of China, Beijing, 2000.

[34] Y. N. du, M. L. Zhu, X. Liu, and F. Z. Xuan, "Effect of long-term aging on near-threshold fatigue crack growth of Ni–Cr–Mo–V steel welds," *Journal of Materials Processing Technology*, vol. 226, pp. 228–237, 2015.

[35] Y. N. Du, M. L. Zhu, and F. Z. Xuan, "Transitional behavior of fatigue crack growth in welded joint of 25Cr2Ni2MoV steel," *Engineering Fracture Mechanics*, vol. 144, pp. 1–15, 2015.

[36] M. A. Meyers and H. R. Pak, "Observation of an adiabatic shear band in titanium by high-voltage transmission electron microscopy," *Acta Metallurgica*, vol. 34, no. 12, pp. 2493–2499, 1986.

[37] T. Nicholas, *High Cycle Fatigue: A Mechanics of Materials Perspective*, Elsevier, San Diego, 2006.